Journal of Fluids and Structures (2002) **16**(7), 971–987
doi:10.1006/jfls.459 available online at http://www.idealibrary.com on IDEAL®

A SIMPLIFIED LINEARIZED MODEL FOR THE FLUID-COUPLED VIBRATIONS OF SPENT NUCLEAR FUEL RACKS

M. Moreira*

Department of Mathematics, School of Technology, Polytechnic Institute of Setubal 2914-508 Setúbal, Portugal,

AND

J. Antunes
Applied Dynamics Laboratory, Institute of Nuclear Technology, 2686-953 Sacavém Portugal

(Received 25 January 2001; and in final form 28 January 2002)

Fluid effects can induce strong coupling between immersed spent nuclear fuel racks, when they are subjected to earthquake excitations. Broc and co-workers found that such system can display two-dimensional vibratory responses, even when external excitations are applied along a symmetry axis of the system. Their analysis was supported by numerical computations, using a finite element code developed at CEA (Saclay) which is well suited for fluid–structure-coupled systems. The present paper was inspired by their work as a possible lighter computational alternative. Here we develop a theoretical model which enables the computation of fluid-coupling effects, subject to some simplifying assumptions: (i) three-dimensional flow effects are neglected, (ii) gaps between the fuel assemblies (and between these and the container) are small when compared with longitudinal length-scales. From these assumptions, we postulate a simplified flow inside the channels, such that gap-averaged velocity and pressure fields are described in terms of a single space coordinate for each fluid channel. Using this approach, the flow can be formulated in analytical terms, enabling effective computation of the dynamical response, of a multi-rack fluid-coupled system.

1. INTRODUCTION

Understanding the complex dynamic behavior of immersed spent-fuel assembly storage racks under earthquake conditions is of prime importance for the safety of nuclear plant facilities.

Fluid effects can induce strong coupling between immersed nuclear fuel racks, when they are subjected to earthquake excitations [see for instance, Stabel *et al*. (1993) or Broc *et al*. (2000)]. Here, we develop a simplified theoretical model which enables the computation and understanding of the fluid-coupling forces. Our simplified model does not take into account friction sliding, uplifting or sloshing effects. As noted by Broc *et al*.

*Visiting researcher at ITN/ADL (Instituto Tecnológico e Nuclear), Sacavém

0889-9746/02/070971 + 17 $35.00/0

(2000), sloshing effects can be neglected because usually there is a large depth of water over the racks in storage pools. Our formulation is subject to the following additional simplifying assumptions: (i) three-dimensional flow effects are neglected, (ii) gaps between the fuel assemblies and between these and the container are small when compared with longitudinal length-scales.

The simplified flow model proposed in the present work is much less computer-intensive than finite element formulations. Hence, the modal behavior and the vibratory responses of the linearized system can be obtained without extensive programming effort. Other advantages of the present approach include the easy integration of dissipative effects, as well as a straightforward extension to address nonlinear flow terms.

2. MODEL FORMULATION

2.1. Fluid Formulation

Consider a pool with $M \times N$ nuclear spent fuel racks arranged in M lines and N columns, which will be identified using matrix notation.

The dimensions along the principal directions of each rack are L_X and L_Y. The Y- and X-direction channels (between each pair of racks or between a wall and a rack) are denoted as

$$H_j^Y, 1 \leq j \leq N+1 \ (Y\text{-direction channel}), \tag{1}$$

$$H_i^X, 1 \leq i \leq M+1 \ (X\text{-direction channel}). \tag{2}$$

In Figure 1 one can see the main geometrical parameters, for a quite general system configuration.

The absolute positions of each rack $(\tilde{X}_{ij}(t), \tilde{Y}_{ij}(t))$ can be defined as

$$\tilde{X}_{ij}(t) = X_{ij}^0 + X_{ij}(t), \qquad \tilde{Y}_{ij}(t) = Y_{ij}^0 + Y_{ij}(t), \tag{3,4}$$

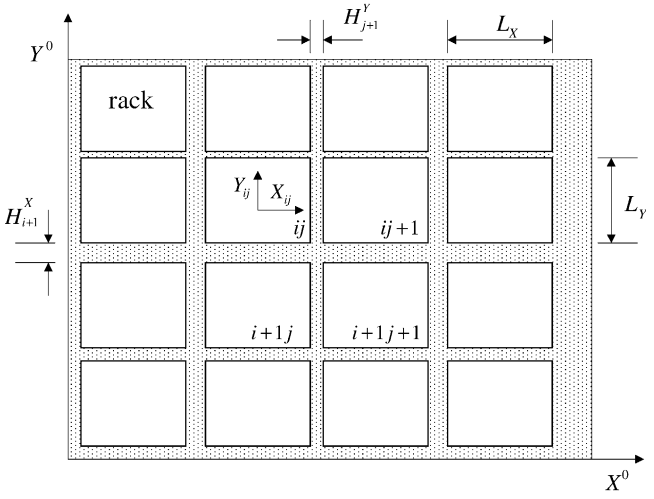

Figure 1. Main geometrical parameters.

where (X_{ij}^0, Y_{ij}^0) are the coordinates of the geometric centers with respect to the pool container and $(X_{ij}(t), Y_{ij}(t))$ are the local coordinates of each rack. So, the actual X-direction $h^X$and Y-direction gaps h^Y, can be defined as

$$h_{ij}^X = H_i^X + Y_{i-1j} - Y_{ij}, \quad \text{for } 1 \le i \le M+1 \quad \text{and} \quad 1 \le j \le N \tag{5}$$

and

$$h_{ij}^Y = H_j^Y + X_{ij} - X_{ij-1}, \quad \text{for } 1 \le i \le M \quad \text{and} \quad 1 \le j \le N+1, \tag{6}$$

where

$$Y_{0j} = Y_{M+1j} = X_{i0} = X_{iN+1} = 0$$

by definition.

Following Antunes *et al.* (1996, 2001), a simplified flow model inside the vertical and horizontal channels can be developed assuming that (i) three-dimensional flow effects are neglected and (ii) the gaps between the fuel assemblies and between these and the walls are small when compared with the longitudinal length-scales. With this approach the flow inside each channel can be modelled as being parallel and we can neglect the transverse gradient in the pressure. We define a gap-averaged velocity as

$$u(z,t) = \frac{\int_0^{h(t)} v_z(z,w,t)\,\mathrm{d}w}{h(t)},$$

where z, w and v_z stand, respectively, for the spatial coordinate along the channel length, the transverse spatial coordinate and the corresponding component of the flow velocity. The continuity equation, in each channel, can be formulated as

$$\frac{\partial h}{\partial t} + \frac{\partial}{\partial z}(uh) = 0, \tag{7}$$

where $u = u(z,t)$ and $h = h(t)$ stand, respectively, for the gap-averaged fluid velocity and the channel gap. Observing similar arguments and the following additional simplification

$$u^2 h \approx \int_0^h [v_z(z,w,t)]^2\,\mathrm{d}w,$$

the momentum equation in each channel, can be written as

$$\rho\left[\frac{\partial}{\partial t}(uh) + \frac{\partial}{\partial z}(u^2 h)\right] + \tau + h\frac{\partial p}{\partial z} = 0, \tag{8}$$

where $p = p(z,t)$ stand for the pressure and τ accommodates all the dissipative effects.

In this paper the dissipative stresses τ are postulated to be of viscous nature,

$$\tau = \alpha u, \tag{9}$$

where α is a proportionality constant. A minimal realistic value for this parameter, α can be approximated relating it with the fluid dynamic viscosity μ and the average channel gap. For instance, assuming a parallel channel parabolic velocity profile V, satisfying [see Richardson (1989)]

$$v(w) = -K\frac{H}{2\mu}w\left(1 - \frac{w}{H}\right), \tag{10}$$

where K, μ and H stand, respectively, for a constant, the dynamic viscosity and the average channel gap, one can deduce, comparing $2\mu(\mathrm{d}V/\mathrm{d}u)|_{w=0}$ and αu,

$$\alpha = 12\frac{\mu}{H}. \tag{11}$$

Using classical perturbation analysis and recalling equations (5) and (6) in which the actual channel gap is separated into a steady term (mean gap) and small fluctuating term, one can linearize the Navier–Stokes equations (7) and (8) about the mean gap. So, equation (7), after linearization and integration, can be written for the Y- and X-direction channels as

$$u_{ij}^X(x,t) = -\frac{(\dot{Y}_{i-1j} - \dot{Y}_{ij})}{H_i^X}x + C_{ij}^X(t), \quad \text{for } 1 \le i \le M+1 \quad \text{and} \quad 1 \le j \le N, \tag{12}$$

$$u_{ij}^Y(y,t) = -\frac{(\dot{X}_{ij} - \dot{X}_{ij-1})}{H_j^Y}y + C_{ij}^Y(t), \quad \text{for } 1 \le i \le M \quad \text{and} \quad 1 \le j \le N+1, \tag{13}$$

where C_{ij}^X and C_{ij}^Y are functions of time stemming from the integration.

Also, linearized forms of equation (8) can be deduced for the X- and Y-direction channels:

$$\rho\dot{u}_{ij}^X H_i^X + \alpha u_{ij}^X + H_i^X\frac{\partial p_{ij}^X}{\partial x} = 0, \quad \text{for } 1 \le i \le M+1 \quad \text{and} \quad 1 \le j \le N, \tag{14}$$

$$\rho\dot{u}_{ij}^Y H_j^Y + \alpha u_{ij}^Y + H_j^Y\frac{\partial p_{ij}^Y}{\partial y} = 0, \quad \text{for } 1 \le i \le M \quad \text{and} \quad 1 \le j \le N+1, \tag{15}$$

where p_{ij}^X and p_{ij}^Y are the pressures in X- and Y-direction channels.

Integration of equations (14) and (15) yields

$$\begin{aligned} p_{ij}^X(x,t) = &-\rho\frac{1}{2}\frac{(\ddot{Y}_{ij} - \ddot{Y}_{i-1j})}{H_i^X}x^2 - \rho\dot{C}_{ij}^X(t)x - \alpha\frac{1}{2}\frac{(\dot{Y}_{ij} - \dot{Y}_{i-1j})}{[H_i^X]^2}x^2 - \alpha\frac{C_{ij}^X(t)}{H_i^X}x \\ &+ p_{ij}^X(0,t), \\ &\text{for } 1 \le i \le M+1 \quad \text{and} \quad 1 \le j \le N \end{aligned} \tag{16}$$

and

$$\begin{aligned} p_{ij}^Y(y,t) = &-\rho\frac{1}{2}\frac{(\ddot{X}_{ij-1} - \ddot{X}_{ij})}{H_j^Y}y^2 - \rho\dot{C}_{ij}^Y(t)y - \alpha\frac{1}{2}\frac{(\dot{X}_{ij-1} - \dot{X}_{ij})}{[H_j^Y]^2}y^2 - \alpha\frac{C_{ij}^Y(t)}{H_j^Y}y \\ &+ p_{ij}^Y(0,t), \\ &\text{for } 1 \le i \le M \quad \text{and} \quad 1 \le j \le N+1. \end{aligned} \tag{17}$$

The X- and Y-direction fluid forces acting (per unit length) on each rack can be found as follows:

$$F_{ij}^X(t) = \int_{-L_Y/2}^{L_Y/2}[p_{ij}^Y(y,t) - p_{ij+1}^Y(y,t)]\,\mathrm{d}y,$$

$$F_{ij}^Y(t) = \int_{-L_X/2}^{L_X/2}[p_{i+1j}^X(x,t) - p_{ij}^X(x,t)]\,\mathrm{d}x,$$

for $1 \le i \le M$ and $1 \le j \le N$, that is,

$$F_{ij}^X(t) = \left(-\rho\frac{(\ddot{X}_{ij-1} - \ddot{X}_{ij})}{H_j^Y} - \alpha\frac{(\dot{X}_{ij-1} - \dot{X}_{ij})}{[H_j^Y]^2}\right)\frac{L_Y^3}{24}$$
$$+ \left(\rho\frac{(\ddot{X}_{ij} - \ddot{X}_{ij+1})}{H_{j+1}^Y} + \alpha\frac{(\dot{X}_{ij} - \dot{X}_{ij+1})}{[H_{j+1}^Y]^2}\right)\frac{L_Y^3}{24}$$
$$+ (p_{ij}^Y(0,t) - p_{ij+1}^Y(0,t))L_Y,$$
$$\text{for } 1 \le i \le M \quad \text{and} \quad 1 \le j \le N, \tag{18}$$

and

$$F_{ij}^Y(t) = \left(-\rho\frac{(\ddot{Y}_{i+1j} - \ddot{Y}_{ij})}{H_{i+1}^X} - \alpha\frac{(\dot{Y}_{i+1j} - \dot{Y}_{ij})}{[H_{i+1}^X]^2}\right)\frac{L_X^3}{24}$$
$$+ \left(\rho\frac{(\ddot{Y}_{ij} - \ddot{Y}_{i-1j})}{H_i^X} + \alpha\frac{(\dot{Y}_{ij} - \dot{Y}_{i-1j})}{[H_i^X]^2}\right)\frac{L_X^3}{24}$$
$$+ (p_{i+1j}^X(0,t) - p_{ij}^X(0,t))L_X,$$
$$\text{for } 1 \le i \le M \quad \text{and} \quad 1 \le j \le N. \tag{19}$$

Note that in equations (16)–(19)

$$\ddot{X}_{ij} = \dot{X}_{ij} = 0, \quad \text{if } i = 0 \text{ or } i = M+1$$

and

$$\ddot{Y}_{ij} = \dot{Y}_{ij} = 0, \quad \text{if } j = 0 \text{ or } j = N+1,$$

as $(X_{ij}(t), Y_{ij}(t))$ are the relative coordinates of each rack.

Note also that, as a consequence of gap intersection effects, the velocity and pressure expressions corresponding to equations (12), (13), (16) and (17) apply only at some distance from the inlets/outlets. These singular dissipative effects could be modelled by pressure drops at the gap intersections, however with a consequent increase in the model complexity. For the purposes of our linearized approach, the linearized inlet/outlet losses may be included through the global coefficient α in the empirical loss term $\tau = \alpha u$.

2.2. Formulation of the Coupled System

Assuming that the racks are linear systems with structural mass M_s, damping C_s and stiffness K_s, all these parameters being per unit length, one can deduce the following fluid–structure model:

$$M_s\ddot{X}_{ij} + C_s\dot{X}_{ij} + K_sX = F_{ij}^X(t) + F_{ij,\text{aut}}^X, \tag{20}$$

$$M_s\ddot{Y}_{ij} + C_s\dot{Y}_{ij} + K_sY = F_{ij}^Y(t) + F_{ij,\text{aut}}^Y, \tag{21}$$

for $1 \le i \le M$ and $1 \le j \le N$ where $F_{ij,\text{aut}}^X$ and $F_{ij,\text{aut}}^Y$ represent external autonomous forces per unit length. Here, the structural parameters have been assumed identical for both directions. However, dealing with asymmetrical systems brings no further difficulties whatsoever.

2.3. Formulation of the Complete system

Note that the $2 \times M \times N$ equations (20) and (21) generated by this approach are not sufficient to find all the corresponding unknowns which are summarized in Table 1. However, between rack or rack/wall positions ij, $ij+1$, $i+1j$ and $i+1j+1$, one can establish the additional equations we need: $(M+1) \times (N+1) - 1$ linearly independent equations of compatibility of flow (mass conservation for all nodes but one), $4 \times M \times N - (M-1) \times (N-1)$ linearly independent equations of compatibility of pressure (in all corners of each rack except $(M-1) \times (N-1)$ corners) and finally, one last equation setting a reference for the pressure.

Here are the compatibility equations of the flow

$$\begin{aligned}&[(\dot{X}_{i+1j+1} - \dot{X}_{i+1j})L_Y - 2H^Y_{j+1}C^Y_{i+1j+1}]\\ &+ [(\dot{Y}_{ij+1} - \dot{Y}_{i+1j+1})L_X + 2H^X_{i+1}C^X_{i+1j+1}(t)]\\ &+ [(\dot{X}_{ij+1} - \dot{X}_{ij})L_Y + 2H^Y_{j+1}C^Y_{ij+1}(t)]\\ &+ [(\dot{Y}_{ij} - \dot{Y}_{i+1j})L_X - 2H^X_{i+1}C^X_{i+1j}(t)] = 0,\end{aligned} \tag{22}$$

for $0 \le i \le M$ and $0 \le j \le N$. Note that we must disregard one of these equations in order to obtain a set of $(M+1) \times (N+1) - 1$ linearly independent equations. In fact, the flow in a corner is completely determined by the flow in the remaining corners.

The equations of compatibility of pressure establish the following $4 \times M \times N - (M-1) \times (N-1)$ relations

$$p^X_{ij}(-L_X/2, t) = p^Y_{ij}(-L_Y/2, t), \tag{23}$$

$$p^X_{ij}(L_X/2, t) = p^Y_{ij+1}(-L_Y/2, t), \tag{24}$$

$$p^X_{i+1j}(-L_X/2, t) = p^Y_{ij}(L_Y/2, t), \tag{25}$$

for $1 \le i \le M$ and $1 \le j \le N$, and

$$p^X_{i+1j}(L_X/2, t) = p^Y_{i+1j+1}(-L_Y/2, t), \tag{26}$$

for $i = M$ and $1 \le j \le N$, and for $1 \le i \le M-1$ and $j = N$.

Table 1
Number of unknowns

Unknowns	Number
$X_{ij}(t)$	MN
$Y_{ij}(t)$	MN
$C^h_{ij}(t)$	$(M+1)N$
$C^v_{ij}(t)$	$M(N+1)$
$p^h_{ij}(0, t)$	$(M+1)N$
$p^v_{ij}(0, t)$	$M(N+1)$
Total	$6MN + 2(M+N)$

Finally,

$$\sum_{\substack{i=1,M+1\\ j=1,N}} p_{ij}^{X}(0,t) + \sum_{\substack{i=1,M\\ j=1,N+1}} p_{ij}^{Y}(0,t) = 0 \tag{27}$$

sets a reference for the pressure.

Again, observe that in equations (22)–(26), the following parameters must be

$$\ddot{X}_{ij} = \dot{X}_{ij} = 0, \quad \text{if } i = 0 \text{ or } i = M+1 \text{ and}$$

$$\ddot{Y}_{ij} = \dot{Y}_{ij} = 0, \quad \text{if } j = 0 \text{ or } j = N+1.$$

In Table 2, we summarize the above-mentioned equations defining our linearized model for the fluid-coupled vibratory responses of the system.

All these equations represent a set of differential–algebraic equations (DAEs). That is, among those equations, some of them are pure algebraic constraints between unknowns. Clearly, this is the case of equation (27). Note that this class of equations arises naturally in many applications, but they present numerical and analytical difficulties which do not occur with systems of ordinary differential equations (Brenan *et al*. 1988). In our case the DAEs developed can be classified as a linear constant-coefficient differential–algebraic system of equations, which can be shown to be of index one. The *index* is an invariant parameter related to each system of DAEs, which is a "measure" of the singularity of the system and so the degree of the numerical and analytical difficulties presented (Hindmarsh & Petzold 1988). The higher the index, the more difficult is the DAE system to solve. Fortunately, our model is not a higher-index system (that is, with an index bigger than one).

Note that these equations can be written and established for generic systems of $M \times N$ racks entirely in a symbolic computer environment as was done here for the tested cases. As an illustration, we present in Appendix A the system model for a single rack generated by an automated procedure.

For convenience one can reduce the order of equations (20) and (21) writing them as

$$M_s\dot{Z}_{ij} + C_s Z_{ij} + K_s X_{ij} = F_{ij}^{X}(t) + F_{ij,\text{aut}}^{X}, \tag{28}$$

$$M_s\dot{W}_{ij} + C_s W_{ij} + K_s Y_{ij} = F_{ij}^{Y}(t) + F_{ij,\text{aut}}^{Y}, \tag{29}$$

$$\dot{X}_{ij} - Z_{ij} = 0, \qquad \dot{Y}_{ij} - W_{ij} = 0. \tag{30, 31}$$

TABLE 2

Equations of the linearized model for the fluid-coupled vibratory response of the system

Description	Equation	Number of equations
Coupled system (X)	(18)	MN
Coupled system (Y)	(19)	MN
Compatibility of flow	(20)	$(M+1)(N+1)-1$
Compatibility of pressure	(21)–(24)	$4MN-(M-1)(N-1)$
Reference of pressure	(25)	1
Total		$6MN+2(M+N)$

3. NUMERICAL SIMULATIONS

Define the set of differential–algebraic equations corresponding to our model as

$$\mathbf{F}(\dot{\mathbf{v}}, \mathbf{v}, t) = \mathbf{0}, \tag{32}$$

where $\mathbf{v}$ is the vector of unknowns. The simplest first-order backward difference formula is the implicit Euler method

$$\mathbf{F}\left(\frac{\mathbf{v}_{n+1} - \mathbf{v}_n}{t_{n+1} - t_n}, \mathbf{v}_{n+1}, t_{n+1}\right) = \mathbf{0}, \tag{33}$$

in which equation (32) is approximated by finite differences (Brenan *et al*. 1988). In the present work we used a fourth- and fifth-order generalization of equation (33) coded in MATLAB [see, Roberts (1998)].

All numerical simulations were performed with the main geometrical, physical and modal parameters presented in Tables 3 and 4. The time-step used, $\triangle t = 0{\cdot}005$, was one order of magnitude smaller than $1/(2f_{\max})$, with $f_{\max} \approx 20$ Hz (maximum frequency of interest).

Two main sets of numerical simulations were performed. The first one using a small-storage pool with a single centered rack and the second one using a pool with ten racks regularly stored in 2 lines and 5 columns.

4. RESULTS AND DISCUSSION

The response of single centered rack to an impulsive excitation is displayed in Figure 2. Comparing the frequency response in air $f_s = 2$ Hz, Figure 2(a), and in water $f_{\text{wat}} = 1{\cdot}48$ Hz, Figure 2(b), one finds:

$$\frac{M_{\text{add}}}{M_s} \approx 0{\cdot}825, \tag{34}$$

TABLE 3

Main geometrical parameters for the numerical simulations

L_X (m)	2
L_Y (m)	2
$H_i^h,\ 1 \leq i \leq M+1$ (m)	0·2
$H_j^v,\ 1 \leq j \leq N+1$ (m)	0·2

TABLE 4

Physical and modal parameters for the numerical simulations

Structural mass, M_s (kg)	32 000
Structural damping, C_s (N s/m)	8 000
Structural stiffness, K_s (N/m)	5×10^6
Modal frequency in air, f_s (Hz)	2
Reduced damping in air, ζ	0·01
Rack density (ρ_s/ρ_{wat})	8
Density of glycerol, ($\rho_{\text{gly}}/\rho_{\text{wat}}$)	1·264
Dynamic viscosity of water, μ_{wat} (N s/m^2)	$1{\cdot}2 \times 10^{-3}$
Dynamic viscosity of glycerol, μ_{gly} (N s/m^2)	1·5

where M_{add} stands for the added mass corresponding to the fluid–structure effect. Observe that such a ratio for an immersed centered cylinder presenting the same annular gap and fluid volume (that is with an average gap of $H = 0{\cdot}2$ and with an equivalent diameter $D = (4/\pi)(L + H) - H$) yields

$$\frac{M_{\text{add}}}{M_s} = \frac{\rho_{\text{wat}} D}{\rho_s 2H} = 0{\cdot}813.$$

This quantity is similar to equation (34), as would be expected. Note that the ratio obtained in equation (34) suggests the following relationship for the added mass (per unit length) of a single centered square rack:

$$M_{\text{add}} = \rho \frac{2}{3} \frac{L^3}{H}. \tag{35}$$

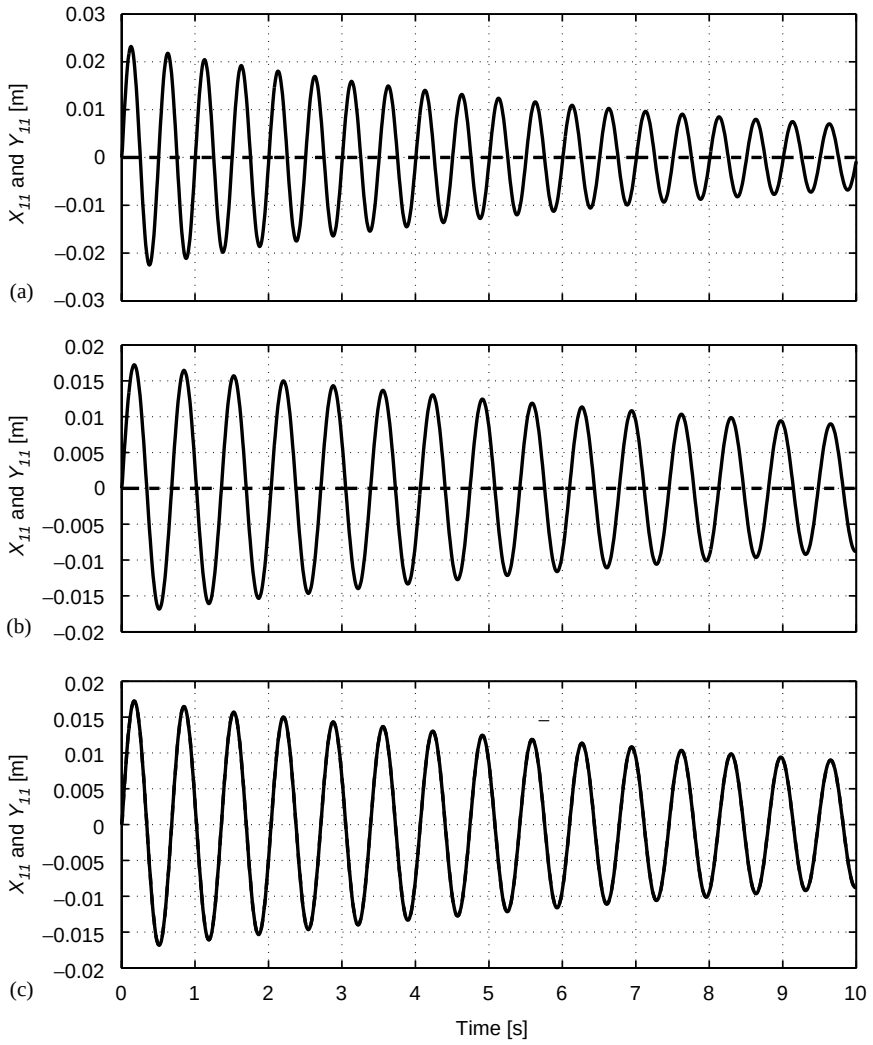

Figure 2. Storage pool with a single rack; responses in direction X (solid) and Y (dashed): (a) response in air to an impulsive force applied in direction X; (b) response in water when the force is applied in direction X; (c) response in water when the force is applied along the rack diagonal.

In fact, equation (35) can be deduced from the system dynamic model for $M = 1$ and $N = 1$, presented in Appendix A, by letting $Y_{11} = \dot{Y}_{11} = \ddot{Y}_{11} = 0$. This can be done by inspecting the coefficient of $\dot{Z}_{11}$ in equation (A3) after substituting the pressure terms by those resulting from equations (A8) and (A9). In these manipulations a time derivative of equation (A5) is fundamental, because it relates $\dot{Z}_{11}$ and $\dot{C}^{Y}_{11}$, as well as the assumption $\dot{C}^{Y}_{11} = \dot{C}^{Y}_{12} = 0$ coming from $Y_{11} = 0$. Similar expressions for the corresponding added mass can be found in Ren & Stabel (1999).

Comparing Figures 2(b) and 2(c), we conclude that the modal response frequency of our system is the same, whether we apply the excitation in direction X or along the rack diagonal. Geometric arguments are in agreement with this fact.

Figure 3 displays the behavior of our system in water letting $\alpha = 0$, Figure 3(a), considering $\alpha = 12\mu_{\text{wat}}/H$, Figure 3(b), and in glycerol with $\alpha = 12\mu_{\text{gly}}/H$, Figure 3(c); i.e., respectively, without fluid dissipative effects (in water) and with dissipative effects in water

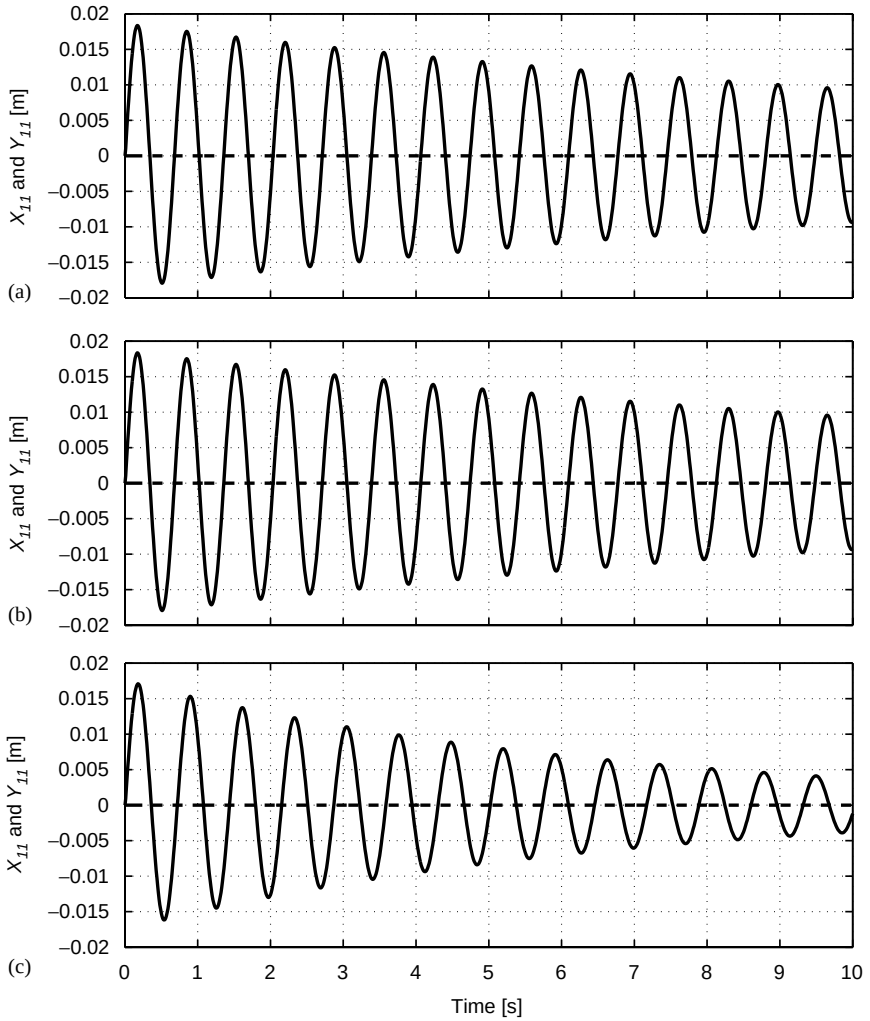

Figure 3. Storage pool with a single rack; response to an impulsive force applied in direction X: (a) $\alpha = 0$; (b) $\alpha = 0{\cdot}072$ (water); (c) $\alpha = 90$ (glycerol). —, Response in the X-direction; - - -, response in the Y-direction.

and glycerol. No significant differences can be detected between 3(a) and 3(b). This means that fluid dissipative effects are not significant for this particular system, in water. It can be shown that only for much lower ratios ρ_s/ρ or much larger fluid viscosities, fluid dissipative effects become significant. Such is the case of our system in glycerol. Note that for this denser fluid, the observed frequency response is only $f_s = 1{\cdot}40$ Hz. This result is consistent with equation (35).

In the next set of numerical simulations, we display the behavior of 10 racks regularly stored in 2 lines and in 5 columns.

In Figure 4, the cumulated spectral responses of the racks to an impulsive excitation applied on rack (1, 1) is displayed: (a) response in air, (b) response in water along direction

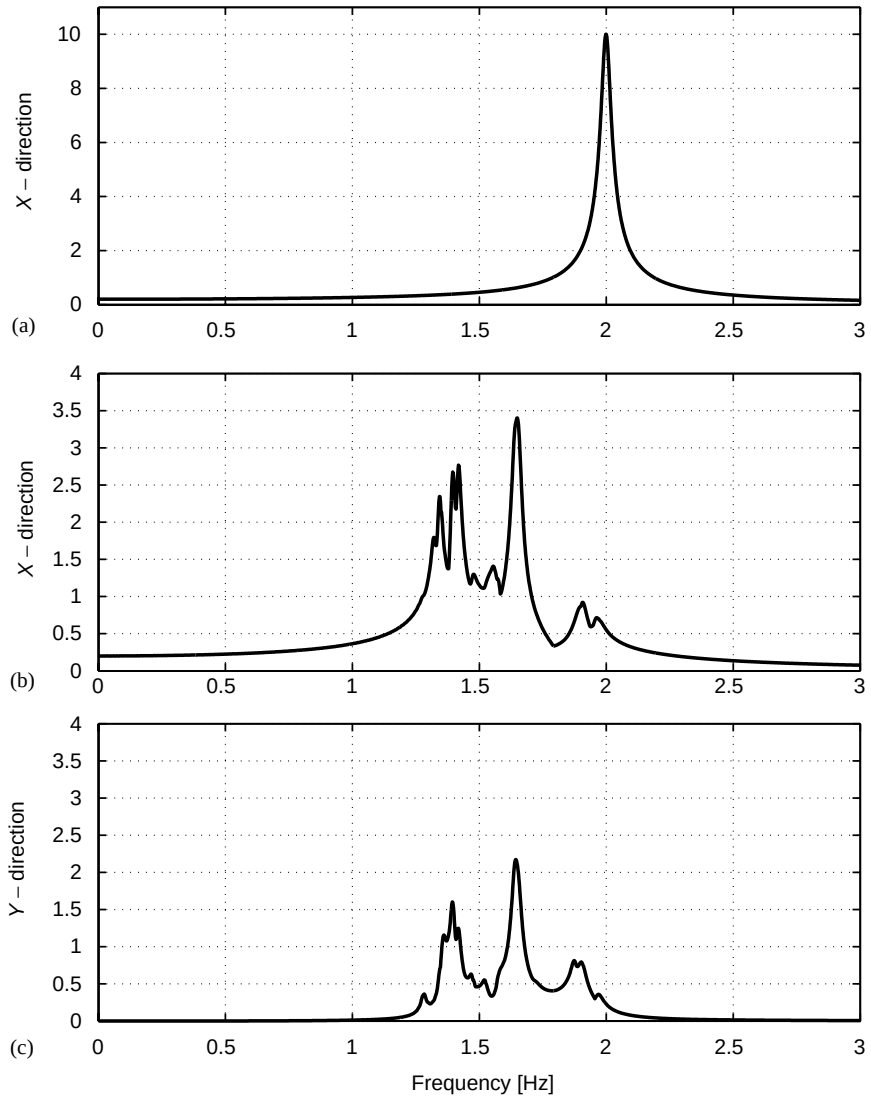

Figure 4. Storage pool with 2×5 racks: Cumulated spectral responses to an impulsive excitation applied on rack (1, 1) along direction X: (a) in air; (b) and (c) in water along each main direction.

X and (c) response in water along direction Y. Letting X_{ij} and Y_{ij} be the time responses of each rack, the cumulated spectral responses can be computed as follows:

$$S^X(\omega) = \max_{ij} (|\mathfrak{F}[X_{ij}(t)]|), \quad S^Y(\omega) = \max_{ij} (|\mathfrak{F}[Y_{ij}(t)]|),$$

where $\mathfrak{F}$ is the Fourier transform, $1 \leq i \leq 2$ and $1 \leq j \leq 5$. Note that, as a result of the applied force, the system displays many different coupled modes in the range between 1 and 2 Hz.

In Figure 5 one can see the (scaled) rack trajectories. All racks display motions in both directions, as a result of the fluid coupling and nonsymmetric excitation.

Finally, in Figure 7, one observes a numerical simulation of the seismic response of our system, to the east–west component of the Loma Prieta earthquake in October 17, 1989. The trace (accelerogram) was taken and supplied by the Natural Sciences Laboratory at U.C. Santa Cruz and is displayed in Figure 6. Again, we display the cumulated spectral response to the above-mentioned excitation applied along the X-direction: (a) computed from the rack responses along direction X and (b) from the rack responses along direction Y, respectively. In spite of the excitation being the same on each rack and only along direction X, we note that the system also exhibits motions perpendicular to this direction. This is accounted for by the presence of a strong fluid–structure interaction. Once can also confirm this fact by observing the (scaled) trajectories of each rack shown in Figure 8. One can notice that, for the computed system, the seismic excitation is mainly "felt" by a particular mode of the rack ensemble. We produced animations of the system response which show clearly that a single mode dominates most of the rack responses, with other modes participating only through the initial transient and final decaying stages of the process.

Note that the symmetry of the responses shown in Figure 8 result by the fact that the seismic excitation was applied along the X-direction (also an axis of symmetry of the storage pool with the racks) and the racks were regularly positioned, letting between them equal channel gaps.

We stress additionally that, in Figures 5 and 8, the trajectories presented were scaled (as we refer in the text) in order to make them observable. In fact, the biggest amplitude verified in those simulations was one order of magnitude smaller than the channel gaps.

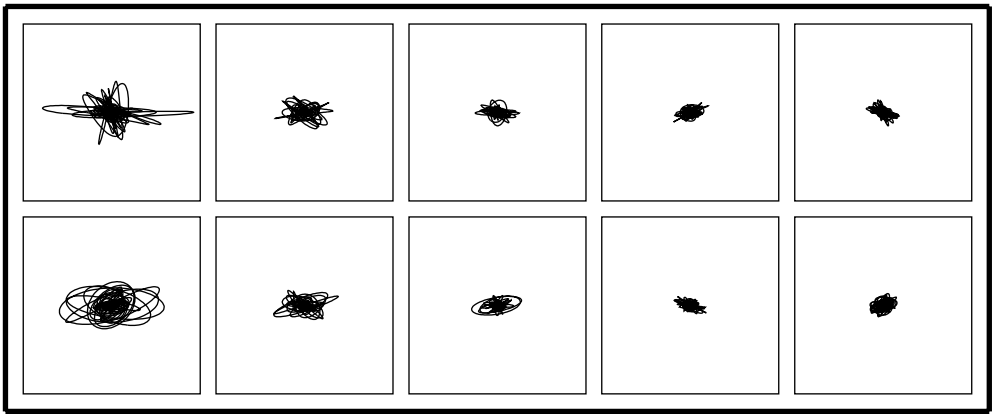

Figure 5. Storage pool with 2×5 racks: scaled trajectories of the racks exhibited as a result of an impulsive excitation applied on rack $(1, 1)$ along direction X.

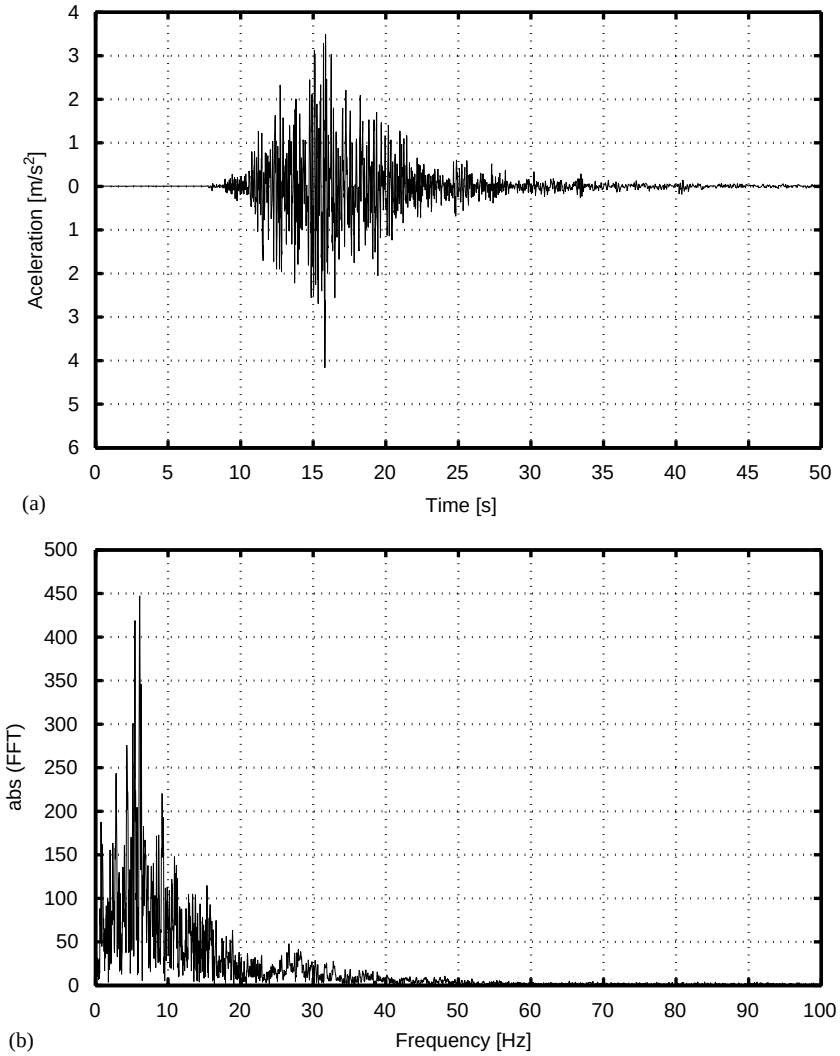

Figure 6. East–west component of the Loma Prieta earthquake in October 17, 1989: (a) excitation accelerogram; (b) the corresponding Fourier transform.

5. CONCLUSIONS

In this paper, we introduced a simplified linearized model for the fluid-coupled vibratory responses of nuclear fuel racks based on the main simplifying assumptions: (i) three-dimensional flow effects were neglected, (ii) gaps between the fuel assemblies and between these and the container are small when compared with the longitudinal length-scales. Using this approach, the flow was analytically formulated in simple terms, enabling effective computation of the dynamical response of a multi-rack fluid-coupled system.

Despite the simplifications introduced, the model developed, yields qualitatively similar predictions when compared with other recently published work [see, Broc *et al.* (2000)].

Besides the fact that the proposed methodology can be automatically implemented on a symbolic computer environment, this model has the following advantages over finite

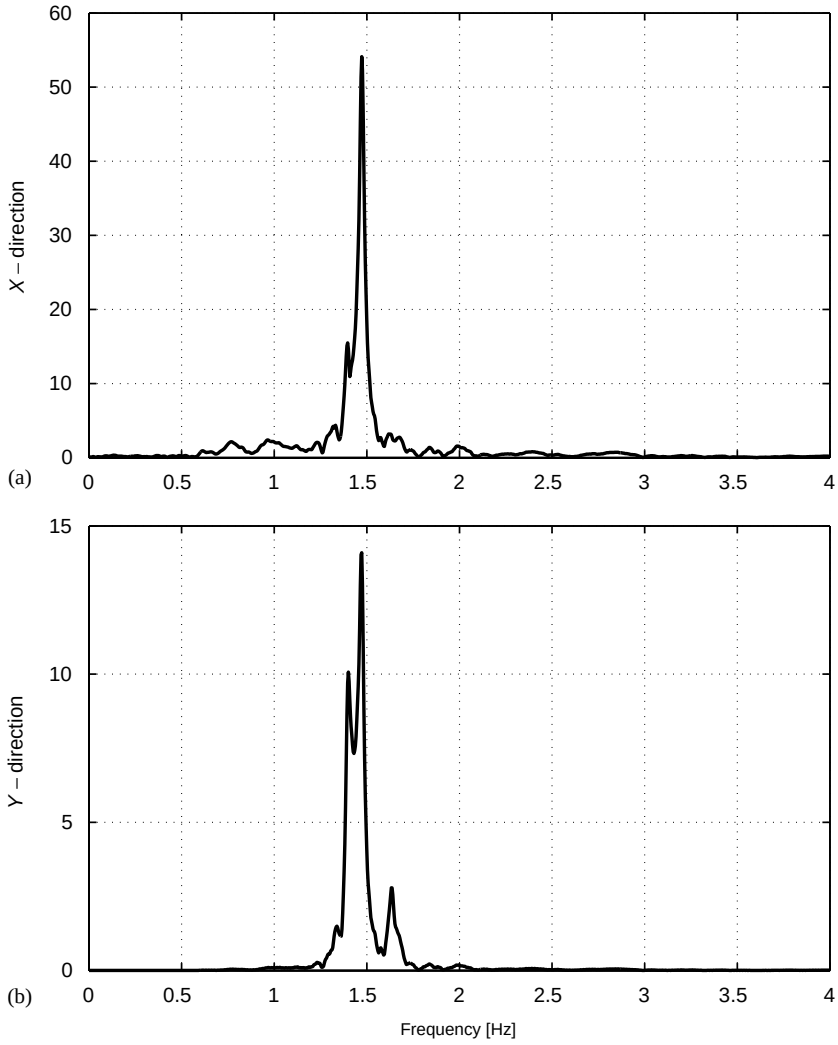

Figure 7. Storage pool with 2×5 racks. Cumulated spectral responses to the seismic excitation applied along direction X: (a) responses along direction X and (b) responses along direction Y.

element approaches: (a) it reduces the number of degrees of freedom of the problem enabling cheaper computations; (b) dissipative effects can be easily considered; (c) generalizations to account for the nonlinear fluid effects, squeeze–film interaction phenomena or even impacts are straightforward; (d) because the fluid model is not very expensive, more realistic computations including frictional rack-supporting forces can be pursued.

Note that, Ren & Stabel (1999) and Stabel & Ren (2001) showed that neglecting three-dimensional flow effects can lead to an overestimation of the true added mass effects. The strategy they use, to account for three-dimensional flow effects, was to introduce flow split factors relating the vertical and the horizontal flows inside the channels between racks, in order to minimize the overall fluid energy.

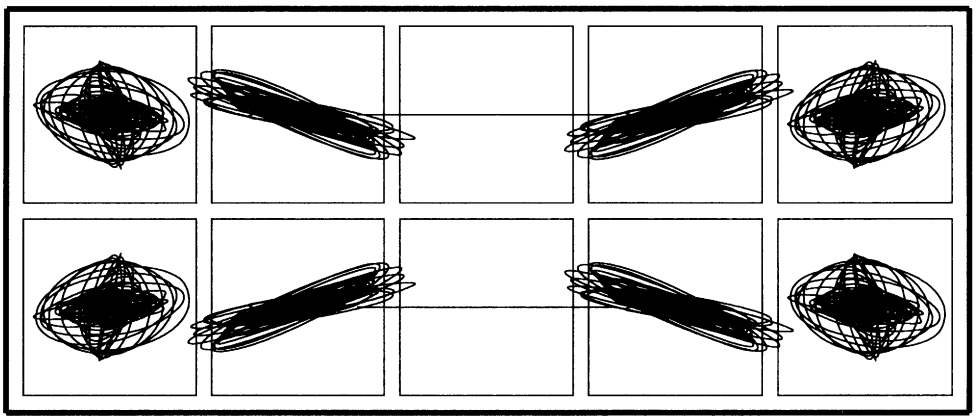

Figure 8. Storage pool with 2×5 racks: scaled trajectories of the racks resulting from a seismic excitation applied along direction X.

The introduction of three-dimensional flow effects into the proposed formulation is currently being addressed. The inclusion of nonlinear extensions and experimental validation is also being prepared.

ACKNOWLEDGEMENTS

Thanks are due to Daniel Broc, from CEA/CEN (Saclay), for useful discussions, which triggered our interest in this problem. Also, we thank the interesting comments and suggestions from Dr Jürgen Stable-Weinheimer, from FRAMATOME ANP.

REFERENCES

ANTUNES, J., AXISA, F. & GRUNENWALD, T. 1996 Dynamics of rotors immersed in eccentric annular flow: Part 1—Theory. *Journal of Fluids and Structures* **10**, 893–918.

ANTUNES, J. & PITEAU, P. 2001 A nonlinear model for squeeze–film dynamics under axial flow. *ASME PVP—Symposium on Flow-Induced Vibration*, Atlanta, PVP Vol. 414-2, pp. 53–62.

BRENAN, K. E., CAMPBELL, S. L. & PETZOLD, L. R. 1996 *Numerical Solution of Initial-Value Problems in Differential–Algebraic Equations*. Philadelphia, PA: SIAM.

BROC, D., QUEVAL J. & CHAUDAT, T. 2000 Fluid–structure interaction for nuclear spent fuel racks. *Emerging Technologies in Fluids*, *Structures and Fluid/Structure Interactions*, *Pressure Vessel and Piping Conference*, Seattle, U.S.A., July 2000, PVP Vol. 414-2, pp. 171–177. New York: ASME.

HINDMARSH, A. C. & PETZOLD, L. R. 1988 Numerical methods for solving ordinary differential equations and differential/algebraic equations. *Energy Technical Review*, September, pp. 23–36.

REN, M. & STABEL, J. 1999 Comparison of different analytical formulations for FSI between fuel storage racks. *Transactions of the 15th International Conference on Structural Mechanics in Reactor Technology* (SMIRT-15), Seoul, Korea, August 15–20.

RICHARDSON, S. C. 1989 *Fluid Mechanics*. Washington, D.C.: Hemisphere Publishing Corporation.

ROBERTS, A. J. 1998 *Differential–Algebraic Equations Solver DAE*. http://www.mathworks.com/support/ftp/diffeqv5.shtml.

STABEL, J. & REN, M. 2001 Fluid–structure interaction for the analysis of the dynamics loads of fuel storage racks in the case of seismic loads. *Nuclear Engineering and Design* **205**, 167–176.

STABEL, J., REN, M & SWELIM, H. 1993 Calculation of seismic loads on fuel storage racks under consideration of fluid–structure interaction, SMiRT-12, pp. 61–66.

APPENDIX A: SYSTEM DYNAMIC MODEL FOR $M = 1$ AND $N = 1$

(a) *Fluid-structural equations*:

$$\dot{X}_{11} - Z_{11} = 0, \qquad \dot{Y}_{11} - W_{11} = 0, \tag{A1, A2}$$

$$\begin{aligned} & M_s \dot{Z}_{11} + C_s Z_{11} + K_s X_{11} - \frac{\rho}{24}\left(\frac{L_Y^3}{H_1^Y} + \frac{L_Y^3}{H_2^Y}\right)\dot{Z}_{11} \\ & - \frac{\alpha}{24}\left(\frac{L_Y^3}{(H_1^Y)^2} + \frac{L_Y^3}{(H_2^Y)^2}\right) Z_{11} - [p_{11}^Y(0,t) - p_{12}^Y(0,t)]L_Y \\ & - F_{11,\text{aut}}^X(t) - F_{\text{sism}}^X(t) = 0, \end{aligned} \tag{A3}$$

$$\begin{aligned} & M_s \dot{W}_{11} + C_s W_{11} + K_s Y_{11} - \frac{\rho}{24}\left(\frac{L_X^3}{H_2^X} + \frac{L_X^3}{H_1^X}\right)\dot{W}_{11} \\ & - \frac{\alpha}{24}\left(\frac{L_X^3}{(H_2^X)^2} + \frac{L_X^3}{(H_1^X)^2}\right) W_{11} - [p_{21}^X(0,t) - p_{11}^X(0,t)]L_X \\ & - F_{11,\text{aut}}^Y(t) - F_{\text{sism}}^Y(t) = 0. \end{aligned} \tag{A4}$$

(b) *Flow compatibility equations*:

$$-L_Y Z_{11} + 2H_1^Y C_{11}^Y + L_X W_{11} - 2H_1^X C_{11}^X = 0, \tag{A5}$$

$$L_Y Z_{11} + 2H_2^Y C_{12}^Y + L_X W_{11} + 2H_1^X C_{11}^X = 0, \tag{A6}$$

$$-L_Y Z_{11} - 2H_1^Y C_{11}^Y - L_X W_{11} - 2H_2^X C_{21}^X = 0. \tag{A7}$$

(c) *Pressure compatibility equations*:

$$\begin{aligned} & -\frac{\rho L_X^2}{8H_1^X}\dot{W}_{11} - \frac{\alpha L_X^2}{8(H_1^X)^2} W_{11} - \frac{\rho L_Y^2}{8H_1^Y}\dot{Z}_{11} - \frac{\alpha L_Y^2}{8(H_1^Y)^2} Z \\ & + \frac{\rho L_X}{2}\dot{C}_{11}^X + \frac{\alpha L_X}{2H_1^X} C_{11}^X + \frac{\rho L_Y}{2}\dot{C}_{11}^Y + \frac{\alpha L_Y}{2H_1^Y} C_{11}^Y \\ & + p_{11}^X(0,t) - p_{11}^Y(0,t) = 0, \end{aligned} \tag{A8}$$

$$\begin{aligned} & -\frac{\rho L_X^2}{8H_1^X}\dot{W}_{11} - \frac{\alpha L_X^2}{8(H_1^X)^2} W_{11} + \frac{\rho L_Y^2}{8H_2^Y}\dot{Z}_{11} + \frac{\alpha L_Y^2}{8(H_2^Y)^2} Z \\ & - \frac{\rho L_X}{2}\dot{C}_{11}^X - \frac{\alpha L_X}{2H_1^X} C_{11}^X + \frac{\rho L_Y}{2}\dot{C}_{12}^Y + \frac{\alpha L_Y}{2H_2^Y} C_{11}^Y \\ & + p_{11}^X(0,t) - p_{12}^Y(0,t) = 0, \end{aligned} \tag{A9}$$

$$\begin{aligned} & \frac{\rho L_X^2}{8H_2^X}\dot{W}_{11} + \frac{\alpha L_X^2}{8(H_2^X)^2} W_{11} - \frac{\rho L_Y^2}{8H_1^Y}\dot{Z}_{11} - \frac{\alpha L_Y^2}{8(H_1^Y)^2} Z \\ & + \frac{\rho L_X}{2}\dot{C}_{21}^X + \frac{\alpha L_X}{2H_2^X} C_{21}^X - \frac{\rho L_Y}{2}\dot{C}_{11}^Y - \frac{\alpha L_Y}{2H_1^Y} C_{11}^Y \\ & + p_{21}^X(0,t) - p_{11}^Y(0,t) = 0, \end{aligned} \tag{A10}$$

$$\frac{\rho L_X^2}{8H_2^X}\dot{W}_{11} + \frac{\alpha L_X^2}{8(H_2^X)^2}W_{11} + \frac{\rho L_Y^2}{8H_2^Y}\dot{Z}_{11} + \frac{\alpha L_Y^2}{8(H_2^Y)^2}Z$$

$$-\frac{\rho L_X}{2}\dot{C}_{21}^X - \frac{\alpha L_X}{2H_2^X}C_{21}^X - \frac{\rho L_Y}{2}\dot{C}_{12}^Y - \frac{\alpha L_Y}{2H_2^Y}C_{12}^Y$$

$$+ p_{21}^X(0,t) - p_{12}^Y(0,t) = 0. \tag{A11}$$

(d) *Pressure reference equation*:

$$p_{11}^X(0,t) + p_{21}^X(0,t) + p_{11}^Y(0,t) + p_{12}^Y(0,t) = 0. \tag{A12}$$

APPENDIX B: NOMENCLATURE

$C_{ij}^X(t), C_{ij}^Y(t)$	fluctuating terms of the fluid velocity
C_s	structural damping per unit length
f_s	structural frequency in the air
$F_{ij,\text{aut}}^X, F_{ij,\text{aut}}^Y$	X- and Y-direction external forces
F_{ij}^X, F_{ij}^Y	X- and Y-direction fluid-elastic forces
X, Y	subscripts for X- and Y-direction channels
$h_{ij}^X(t), h_{ij}^Y(t)$	actual channel gaps
H, H_i^X, H_j^Y	average channel gaps
i, j	line and column subscripts
K_s	structural stiffness per unit length
L, L_X, L_Y	main dimensions of each rack
M_{add}	fluid added mass per unit length
M_s	structural mass per unit length
$p_{ij}^X(y,t), p_{ij}^Y(x,t)$	gap-averaged pressures
t	time
$u_{ij}^X(y,t), u_{ij}^Y(x,t)$	gap-averaged fluid velocities
$X_{ij}(t), Y_{ij}(t)$	relative rack motions
x, y	spatial coordinates along the horizontal and vertical channels
$X_{ij}^0(t), Y_{ij}^0(t)$	rack positions with respect to the pool container
$\tilde{X}_{ij}(t), \tilde{Y}_{ij}(t)$	absolute positions of the racks
z, w	generic longitudinal and transverse spatial coordinates
$Z_{ij}(t), W_{ij}(t)$	time derivative of rack motions
α	damping parameter
μ	dynamic viscosity of the fluid
ρ	fluid density
ρ_s	rack density